COMPUTATIONAL PROBLEMS OF ELECTRICAL ENGINEERING

Vol. 2, No. 2, 2012

INDUCTION SHRINK FITS FOR CONNECTING DISKS AND SHAFTS

Václav Kotlan, Bohuš Ulrych, Ivo Doležel
University of West Bohemia, Czech Republic
{vkotlan, ulrych, idolezel}@kte.zcu.cz

Abstract: A complete model of the induction shrink fit between a disk and shaft is presented. The model consists of a proposal of appropriate interference, checking the von Mises stress in the disk and shaft, mapping of the process of induction heating and determining the release revolutions. The methodology is illustrated by a typical example.

Key words: induction shrink fit, magnetic field, temperature field, field of thermoelastic displacements, finite element analysis.

1. Introduction

Shrink fit is a firm connection of two metal parts based on the principle of elastic stress. Its task is usually to transfer mechanical forces or torques. This kind of fit finds wide applications in many industrial, transport and other technologies. We can mention, for example, crankshafts, shrunk-on rings, armature bandages in various rotating electric machines or tires of railway wheels [1].

The shrink fit between the disk and shaft is realized either by hydraulic pressing or by heating of the disk, its setting on the shaft and cooling of the whole system. In the latter case (which is discussed in this paper) the disk can be heated by gas or inductively. The aim of heating is to enlarge the diameter of its bore to a value greater than the diameter of the shaft. Then the disk is put on the shaft and the whole system is cooled. The process is schematically shown in Fig. 1.

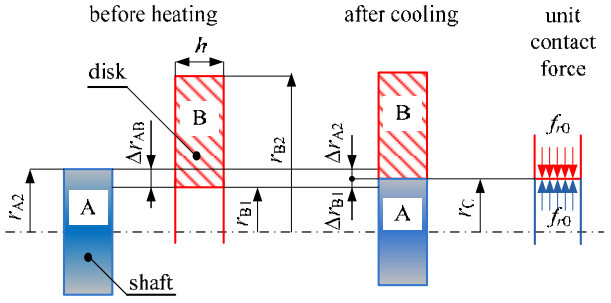

Fig. 1. Preparation of a shrink fit.

The shaft of external radius r_{A2} is manufactured with interference Δr_{AB} with respect to the internal radius r_{B1} of the disk. After heating, the internal radius of the disk must reach a value $r'_{B1} > r_{A2}$. Putting it on the shaft and cooling, the disk shrinks, which leads to the decrease of both radii r_{A2} and r'_{B1} to a common radius r_C that satisfies inequality $r_{B1} < r_C < r_{A2}$ (even the shaft is considered elastic). Shrinking of both parts produces at the place of contact a unit contact force $\pm f_{r0}$ (index 0 means "at rest") between them (see Fig. 1), which allows transferring the mechanical torque.

The paper presents a complete model of the process applied to a disk of a rectangular cross section (but it can easily be extended to a disk of any cross section).

2. Formulation of the technical problem

Consider a shrink fit consisting of a steel disk of dimensions r_{B1}, r_{B2} and h and a shaft of the same material. The fit must be able to safely transfer a prescribed mechanical torque $M_{rn_0\max}$ at the given revolutions n_0. The task is to propose its parameters and check them with respect to the required mechanical properties of the system.

The complete model of the problem consists of four submodels described in the following points:

- Starting from the geometry of the disk and mentioned torque $M_{rn_0\max}$ it is necessary to find sufficient interference Δr_{AB}. This is, however, a very complicated inverse problem. The easiest way is, therefore, to find the dependence $M_{rn\max} = M_{rn\max}(\Delta r_{AB})$ ($M_{rn\max}$ being the maximum transferable torque for the given interference Δr_{AB} within the range of revolutions $n \in \langle 0, n_0 \rangle$) and then to estimate the value Δr_{AB} from this curve.
- Check of the mechanical stress of the disk after its pressing on the shaft. This starts from knowledge of the unit contact force $\pm f_{rn}$ for the whole range of possible revolutions $n \in \langle 0, n_0 \rangle$. This value then serves for computing the reduced stress $\sigma_{\mathrm{red},n}$ (for example, $\sigma_{\mathrm{red},n\mathrm{Mi}}$ by the von Mises hypothesis) and its comparison with the yield stress σ_k of the steel used. For growing revolutions, the effect of the centrifugal forces (acting mainly in the disk) may significantly change the maximum acceptable reduced stress.

- Due to the centrifugal forces, the unit contact force $\pm f_{rn}$ at the place of the contact of both parts decreases with increasing revolutions. A check of the shrink fit has to be performed with respect to the danger of slipping of the disk.
- Determination of the release revolutions n_{rel}. After reaching these revolutions ($n_{\mathrm{rel}} > n_0$) the unit contact force $\pm f_{rn_{\mathrm{rel}}}$ is no longer able to transfer the prescribed torque $M_{rn_0\,\max}$.
- Mapping of the process of induction heating of the disk. Its purpose is to find the parameters of the field current in the inductors (amplitude and frequency) that would secure that the internal radius of the disk reaches a value r'_{B1} in a reasonable time, still acceptable temperature and a good efficiency of the heating process.

3. Continuous mathematical model

The mathematical model of the problem consists of two independent submodels. The first of them is purely mechanical and is intended for finding the unit contact force $\pm f_{rn}$ acting along the contact place on the disk and shaft after pressing for the considered range of revolutions $n \in \langle 0, n_0 \rangle$, corresponding values of the maximum transferable torques $M_{rn\max}$, and also von Mises stresses $\sigma_{\mathrm{red},n\mathrm{Mi}}$.

Provided that these values are acceptable, we apply the second submodel for the description of the process of induction heating. This task represents a nonlinear triply coupled problem characterized by the interaction of magnetic field, temperature field and field of thermoelastic displacements. The physical properties of material are functions of the temperature.

The first (mechanical) submodel is given by the isothermic Lamé equation in the form [2]

$$(\varphi+\psi)\cdot\operatorname{grad}(\operatorname{div}\boldsymbol{u})+\psi\cdot\Delta\boldsymbol{u}+\boldsymbol{f}_{\mathrm{L}}=\boldsymbol{0},$$
$$\varphi=\frac{\nu\cdot E}{(1+\nu)(1-2\nu)},\quad \psi=\frac{E}{2\cdot(1+\nu)}. \qquad (1)$$

Here, E denotes the Young modulus of elasticity of the material, ν is the Poisson coefficient of the contraction, symbol $\boldsymbol{u}=(u_r,u_\varphi,u_z)$ represents the vector of the displacements, and $\boldsymbol{f}_{\mathrm{L}}=(f_{\mathrm{L},r},f_{\mathrm{L},z})$ stands for the vector of the volumetric forces. For the considered axisymmetric arrangement $u_\varphi=0$, and (neglecting the gravitational forces) $f_{\mathrm{L},z}=0$. The component $f_{\mathrm{L},r}$ is given by the formula for the specific centrifugal force

$$f_{\mathrm{L},r}=\rho r\omega^2,\quad \omega=2\pi n/60, \qquad (2)$$

where ρ denotes the specific mass of the disk.

The boundary conditions to (1) are prescribed in accordance with Fig. 2 (due to symmetry it is sufficient to consider just halves of both parts).

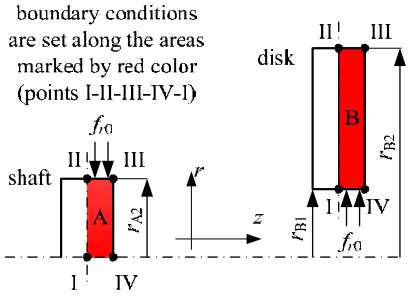

Fig. 2. Determination of the boundary conditions.

- Shaft: edge I-II: $u_z=0,\ f_r=0$, edge II–III: $f_r=-f_{rn},\ f_z=0$, edge III-IV: $f_r=f_z=0$, edge IV-I: $u_r=0,\ f_z=0$.
- Disk: edge I-II: $u_z=0,\ f_r=0$, edge II–III: $f_r=f_z=0$, edge III-IV: $f_r=f_z=0$, edge IV–I: $f_r=f_{rn},\ f_z=0$.

Here, f_r and f_z denote the external forces in the r and z directions, while u_r and u_z denote the displacements in the same directions.

Unfortunately, the unit contact force f_{rn} (see Fig. 1) is not known beforehand. The task must be, therefore, solved iteratively in the following way:

- Choice of unit contact force f_{rn},
- Numerical solution of (1): first for the shaft, second for the disk. Its solution for the shaft provides the displacement Δr_{A2}, solution for the disk provides displacement Δr_{B1}.
- Calculation of $\delta=|\Delta r_{\mathrm{A2}}|+|\Delta r_{\mathrm{B1}}|-|\Delta r_{\mathrm{AB}}|$,
- If $|\delta|<\delta_0$, where δ_0 is a prescribed tolerance, the computations stop, otherwise the value of the unit contact force f_{rn} must be changed appropriately and the system must be recalculated.

After finishing this iterative process, we can easily find the maximum transferable torque $M_{rn\max}$ and also the corresponding von Mises stress $\sigma_{\mathrm{red},n\mathrm{Mi}}$. The relation for the torque $M_{rn\max}$ reads

$$M_{rn\max}=2\pi r_{\mathrm{C}}^2 h|f_{rn}|f_{\mathrm{f}},\quad r_{\mathrm{C}}=r_{\mathrm{B1}}+\Delta r_{\mathrm{B1}}, \qquad (3)$$

where h denotes the width of the disk, r_{C} stands for the final common radius of the shaft and disk (see Fig. 1) and f_{f} is the coefficient of dry friction steel – steel. The von Mises reduced stress $\sigma_{\mathrm{red},n\mathrm{Mi}}$ (in the axisymmetric arrangement) is given by the formula

$$\sigma_{\mathrm{red},n\mathrm{Mi}} = \sqrt{\frac{1}{2}\left[\left(\sigma_r - \sigma_z\right)^2 + \sigma_r^2 + \sigma_z^2\right]}, \qquad (4)$$

where σ_r and σ_z denote the radial and axial stresses at a point, respectively.

The last mechanical task is the determination of the release revolutions n_{rel}. These are given by the condition that the original interference Δr_{AB} between the disk and shaft vanishes due to their deformations δr_{AB} by the centrifugal forces at these revolutions. In such a case $\pm f_{rn_{\mathrm{rel}}} = 0$ and the fit is no longer able to transfer any mechanical torque. The value of δr_{AB} can be determined from the solution of the Lamé equation for the revolutions n. Furthermore, the van Mises stress $\sigma_{\mathrm{red},n_{\mathrm{rel}}\mathrm{Mi}}$ has to be checked as well, because the growing revolutions result in higher stress in the disk.

The second submodel describing the process of induction heating (see Fig. 3) consists of three second-order partial differential equations describing the distribution of the three above mentioned fields.

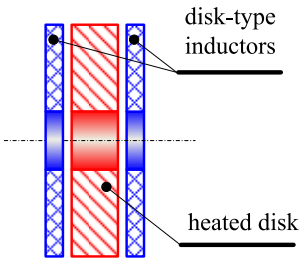

Fig. 3. Induction heating of the disk.

The magnetic field in the system is described by the solution of a well-known parabolic equation for the magnetic vector potential $\boldsymbol{A}$ in the form [3]

$$\mathrm{curl}\left(\frac{1}{\mu}\mathrm{curl}\,\boldsymbol{A}\right) + \gamma\frac{\partial \boldsymbol{A}}{\partial t} = \boldsymbol{J}_{\mathrm{ext}}, \qquad (5)$$

where μ denotes the magnetic permeability, γ stands for the electric conductivity and $\boldsymbol{J}_{\mathrm{ext}}$ is the vector of the external harmonic current density in the field coils.

But a solution to (5) is, in this particular case, practically unfeasible. The reason consists in the deep disproportion between the frequency f (usually tens or hundreds Hz) of the field current I_{ext} and time of heating t_{H} (minutes). That is why the model was somewhat simplified using the assumption that the magnetic field is harmonic. In such a case it can be described by the Helmholtz equation for the phasor $\underline{\boldsymbol{A}}$ of the magnetic vector potential $\boldsymbol{A}$ [3]

$$\mathrm{curlcurl}\,\underline{\boldsymbol{A}} + \mathrm{j}\cdot\omega\gamma\mu\,\underline{\boldsymbol{A}} = \mu\,\underline{\boldsymbol{J}}_{\mathrm{ext}}. \qquad (6)$$

Here, ω denotes the angular frequency ($\omega = 2\pi f$). But the magnetic permeability of ferromagnetic parts needs not be a constant; it can always be assigned to the local value of magnetic flux density. It computation is, in such a case, based on an appropriate iterative procedure.

The conditions along the axes of the system and artificial boundary placed at a sufficient distance from it are of the Dirichlet type ($\underline{\boldsymbol{A}} = \underline{\boldsymbol{0}}$).

The temperature field is described by the heat transfer equation [4]

$$\mathrm{div}\left(\lambda\cdot\mathrm{grad}T\right) = \rho c_{\mathrm{p}}\cdot\frac{\partial T}{\partial t} - p, \qquad (7)$$

where λ is the thermal conductivity, ρ denotes the mass density and c_{p} stands for the specific heat (all of these parameters are generally temperature-dependent functions). Finally, symbol p denotes the time average internal volumetric sources of heat that generally consist of the volumetric Joule losses p_{J} (due to eddy currents) and magnetization losses p_{m}. So we can write

$$p = p_{\mathrm{J}} + p_{\mathrm{m}}, \qquad (8)$$

where

$$p_{\mathrm{J}} = \frac{\left|\underline{\boldsymbol{J}}_{\mathrm{eddy}}\right|^2}{\gamma}, \quad \underline{\boldsymbol{J}}_{\mathrm{eddy}} = \mathrm{j}\cdot\omega\gamma\,\underline{\boldsymbol{A}}, \qquad (9)$$

while p_{m} (if they are considered) are determined from the known measured loss dependence $p_{\mathrm{m}} = p_{\mathrm{m}}\left(\left|\underline{\boldsymbol{B}}\right|\right)$ for the material used (magnetic flux density $\boldsymbol{B}$ in every element is in this model also harmonic).

The boundary conditions take into account convection and radiation.

Finally, the solution of the thermoelastic problem is solved by means of the Lamé nonisothermic equation in the form

$$\begin{aligned}&\left(\varphi+\psi\right)\cdot\mathrm{grad}\left(\mathrm{div}\,\boldsymbol{u}\right) + \psi\cdot\Delta\boldsymbol{u} - \\ &-\left(3\varphi+2\psi\right)\cdot\alpha_{\mathrm{T}}\cdot\mathrm{grad}\,T = \boldsymbol{0}.\end{aligned} \qquad (10)$$

where α_{T} is the coefficient of the linear thermal dilatability of material and T denotes the temperature. Other parameters are identical with those in (1). The boundary conditions correspond to the free disk.

It is important to notice that practically all physical parameters of material of the disk (μ, γ, λ, ρc_{p}, α_{T}) are generally temperature-dependent functions. That is why the problem of induction heating characterised by the interaction of the above three fields cannot be solved in the weak formulation. On the other hand, when the temperature of the disk does not exceed about 300 °C, the magnetic permeability of steel can be considered (with only a very small error) independent of temperature.

4. Numerical computation

The numerical solution of the task was realized by codes QuickField (mechanical submodel) and COMSOL

Multiphysics (induction heating submodel) supplemented with a number of own scripts and procedures. Attention was particularly paid to the convergence of results in the dependence on the density of discretization mesh and distance of the artificial boundary (in case of magnetic field). The results were required to reach 2–3 valid digits. The full computation of one example takes (on a good PC) several hours.

5. Illustrative example

The nominal radii of the shaft and internal bore of the disk $r_{A2} = r_{B1} = 0.1\,\text{m}$, $r_{B2} = 0.5\,\text{m}$, $h = 0.05\,\text{m}$ (see Fig. 1). The interference Δr_{AB} was tested within the range $0 - 0.3\,\text{mm}$. The physical parameters of the disk and shaft manufactured of steel AISI 4130 are known. Some of them γ, λ, ρ, c_p, α_T are temperature-dependent functions and together with the magnetization curve are depicted in Fig. 4–8.

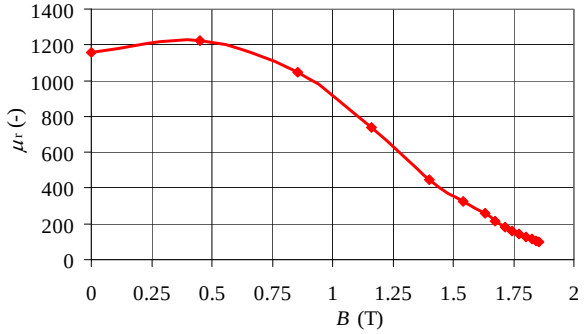

Fig. 4. Magnetisation characteristic of steel AISI 4130 at the room temperature.

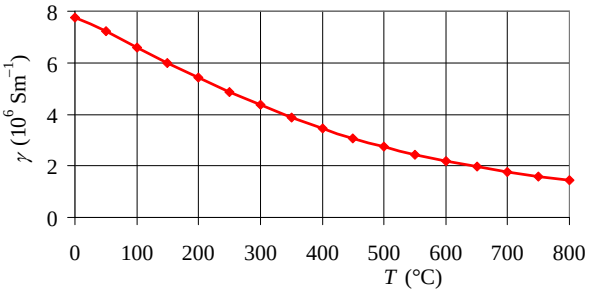

Fig. 5. Temperature dependence of electrical conductivity of steel AISI 4130.

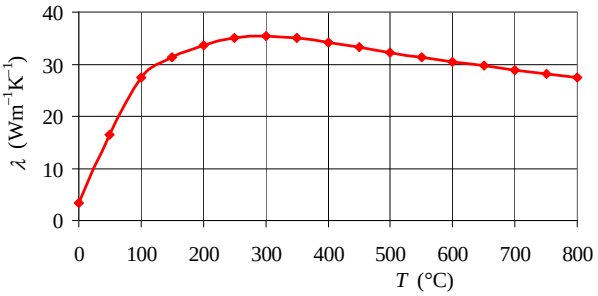

Fig. 6. Temperature dependence of thermal conductivity of steel AISI 4130.

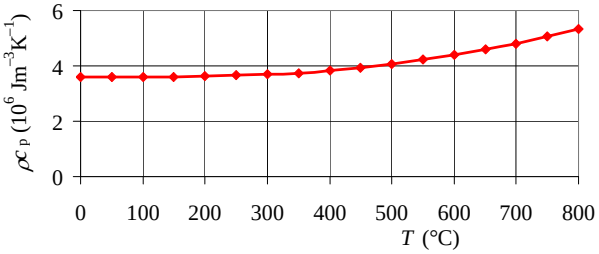

Fig. 7. Temperature dependence of specific heat of steel AISI 4130.

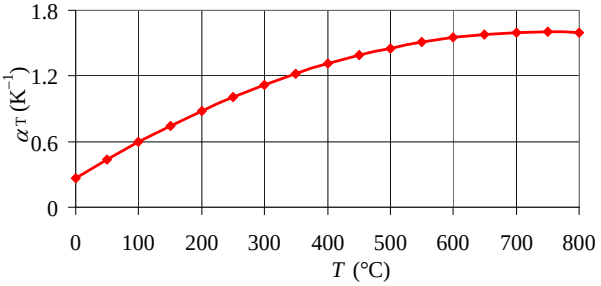

Fig. 8. Temperature dependence of thermal dilatability of steel AISI 4130.

Other parameters are supposed constant ($E = 2.1\times10^{11}\,\text{N/m}^2$, $\nu = 0.3$). The yield stress of steel AISI 4130 $\sigma_k = 4.226\times10^8\,\text{Nm}^{-2}$ and the coefficient of friction $f_f = 0.55$. The nominal mechanical revolutions of the system are $n_0 = 3000\,\text{rev/min}$ and power to be transferred $P = 1\,\text{MW}$, which corresponds to mechanical torque $M_{rn_0} = 3184\,\text{Nm}$.

Fig. 9 shows the dependences of the von Mises stresses in the shaft and disk (at rest, $n = 0$) as functions of the interference Δr_{AB}. Both depicted functions are practically linear. The highest allowable interference for the disk (for which still $\sigma_{red,0Mi} \le \sigma_k$) is 0.22 mm. This value also provides the maximum allowable torque (at rest) $M_{r0\,max} = 4.182\times10^5\,\text{Nm}$ calculated from (2), see Fig. 10.

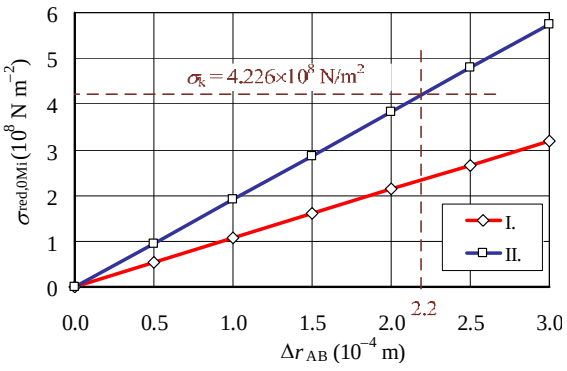

Fig. 9. Von Mises stress $\sigma_{red,0Mi}$ in the system at rest as a function of Δr_{AB} : I – shaft (here $\sigma_{red,0Mi} = f_{r0}$), II – disk.

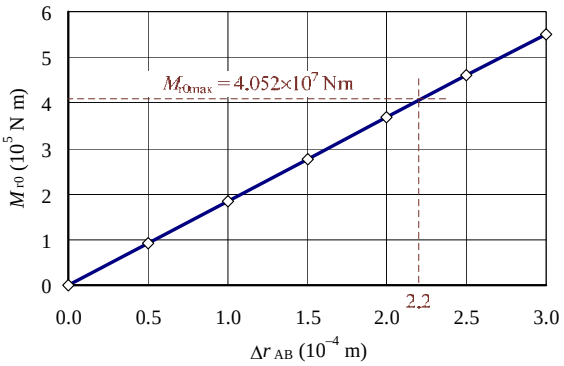

Fig. 10. Transferable torque M_{r0} of the shrink fit (at rest) as a function of Δr_{AB}.

In the next text we will suppose (with regard to the safety of the shrink parameters) that $\Delta r_{AB} = 0.2$ mm.

Fig. 11 shows the dependence of the von Mises stress $\sigma_{red,nMi}$ on revolutions n for $\Delta r_{AB} = 0.2$ mm. Although this stress in the disk slightly increases with the revolutions, yet it does not exceed the yield stress $\sigma_k = 4.226\times10^8$ N/m^2 even after reaching the revolutions $n = 3000$ /min. Analogously, Fig. 12 shows the dependence of the maximum transferable torque $M_{rn\max}$ on the revolutions n. The torque drops from the value 3.7×10^5 Nm at rest to the value 2.3×10^5 Nm at revolutions $n = 3000$ rev min^{-1}, which is still enough for transferring power on the order of 10^7 W.

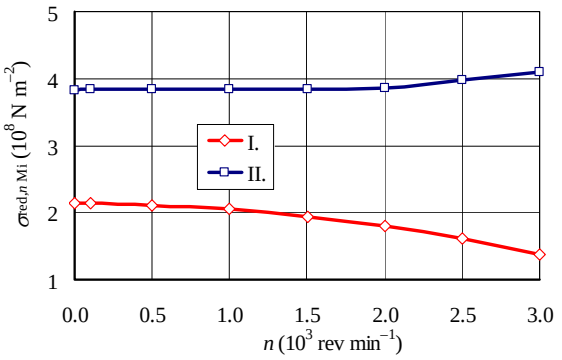

Fig. 11. Dependence of the von Mises stress $\sigma_{red,nMi}$ as a function of revolutions n: I – shaft, II – disk ($\Delta r_{AB} = 0.2$ mm).

Finally, Fig. 13 shows the dependence of the von Mises stress in the disk on its radius both at rest ($n = 0$) and $n_0 = 3000$ rpm, again for $\Delta r_{AB} = 0.2$ mm. This stress strongly drops with the radius, so that there is nowhere a danger of exceeding the yield stress $\sigma_k = 4.226\times10^8$ Nm^{-2} of the used material.

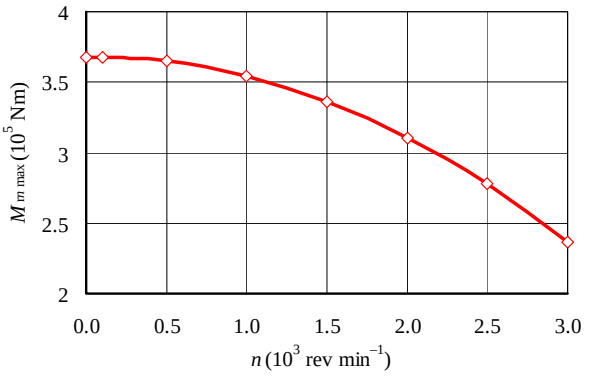

Fig. 12. Dependence of the maximum transferable torque M_{rn} on the revolutions n ($\Delta r_{AB} = 0.2$ mm).

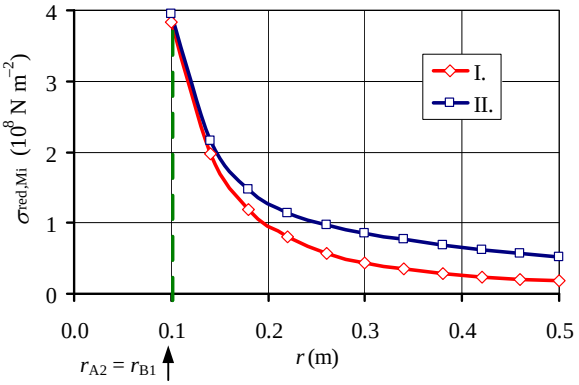

Fig. 13. Dependence of the von Mises stress $\sigma_{red,Mi}$ in the disk on the radius I – at rest ($n = 0$), II – at nominal revolutions $n_0 = 3000$ rpm ($\Delta r_{AB} = 0.2$ mm).

The last two figures from the mechanical part of the task koncern the release revolutions n_{rel}. Fig. 14 shows the dependence of δr_{AB} on the revolutions n, where δr_{AB} denotes the growth of the difference between the inner radius of the disk and radius of the shaft due to deformations brought about by the growing centrifugal forces. As soon as the value of δr_{AB} reaches the value of the interference $\Delta r_{AB} = 0.2$ mm, the contact force $\pm f_{rn}$ vanishes and the fit cannot transfer any mechanical torque. The graph shows that the situation occurs at $n_{rel} \doteq 5030$ rpm.

Fig. 15 contains the dependence of the unit contact force $|f_{rn}|$ acting between the disk and shaft (red line) for growing revolutions n (it decreases to zero for the release revolutions $n_{rel} \doteq 5030$ rpm. The blue line shows, on the other hand, an analogous dependence of the von Mises stress $\sigma_{red,nMi}$ in the disk (along its internal bore) that grows due to growing influence of the centrifugal forces (and in the depicted range it exceeds the yield stress σ_k of the used steel). On the other hand

the fit is not supposed to work at higher revolutions than the nominal ones n_0.

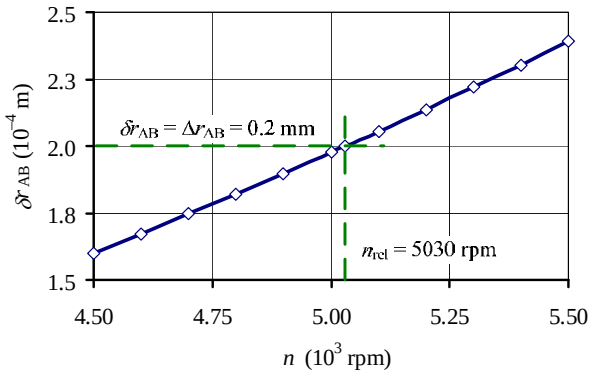

Fig. 14. Dependence of δr_{AB} on revolutions n.

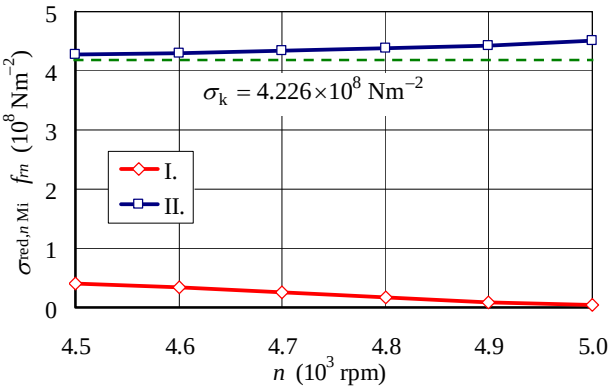

Fig. 15. Dependence of force $|f_{rn}|$ (I) and von Mises stress $\sigma_{red,nMi}$ in the disk (II) on revolutions n.

It is clear that from the mechanical viewpoint the shrink fit satisfies all requirements. The second part of the results concerns the process of induction heating. During the process the disk is placed on a ceramic "shaft" and heated by two disk-type inductors, which is schematically shown in Fig. 16.

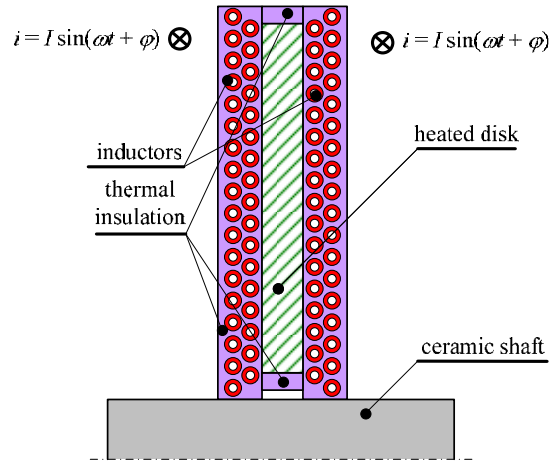

Fig. 16. Realisation of the process of induction heating.

Both inductors made of massive hollow copper conductors cooled by flowing water carry harmonic currents of the same phase shift, thus producing transversal magnetic field in the system. The inductors are placed in a case containing good thermal insulation in order to minimise heat losses. The thermal insulation is placed also between the ceramic shaft and heated disk, as well as slony the external surface of the disk. The process of heating is then almost adiabatic, exhibiting a very favourable efficiency.

The field current parameters were selected in accordance with the possibilities of common industrial plants. While its frequency was set $f = 50$ Hz, its amplitude ranged from $1-3$ kA (such currents are still commonly available). The thermal conductivity of thermal insulation – glass wool – $\lambda = 0.04$ Wm^{-1}K^{-1} and its specific heat $\rho c_{p,gw} = 0.04824\times10^6$ Jm^{-3}K^{-1}. The temperature of the cooling water in the hollow conductors of the inductor $T_w = 50\,°$C.

The boundary conditions along the area containing the disk and inductors placed in thermal insulation are of the convection type (coefficient $\alpha = 20$ Wm^{-2}K^{-1}). The initial temperature of the heated system T_0 is equal to the temperature T_{ext} of the ambient air, which is 30 °C.

Some illustrative results follow. Fig. 17 shows the distribution of magnetic field in the system at the beginning of the heating process, i.e., at the room temperature and Fig. 18 depicts the distribution of the volumetric Joule losses along the surface of the disk (in the r-direction) in different depths for the same case.

It is evident that the volumetric Joule losses are produced mainly in the surface layers of the disk and also in the lower and upper turns of both inductors (where the vectors of magnetic field strongly change thein directions). Thus, the disk is heated mainly at its surface and heat is then conducted to its interior.

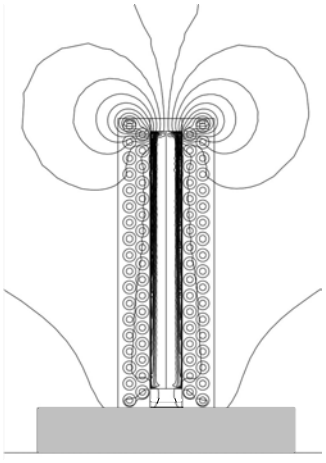

Fig. 17. Distribution of magnetic field in the system at the beginning of the heating process ($T_0 = 30\,°$C, $I = 2.5$ kA).

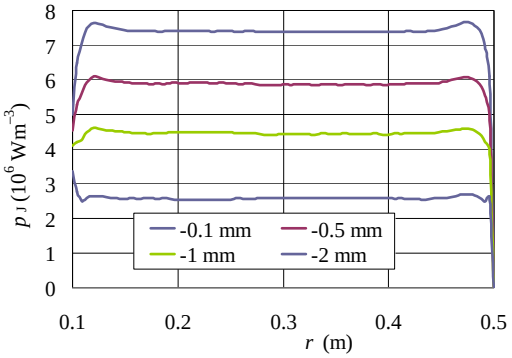

Fig. 18. Distribution of volumetric Joule losses p_J in the disk along its surface in different depths at the beginning of the heating process ($T_0 = 30\,°C$, $I = 2.5$ kA).

For the same current parameters Fig. 19 shows the distribution of temperature in the system in time $t = 1320$ s (22 min) and Fig. 20 the field of displacements.

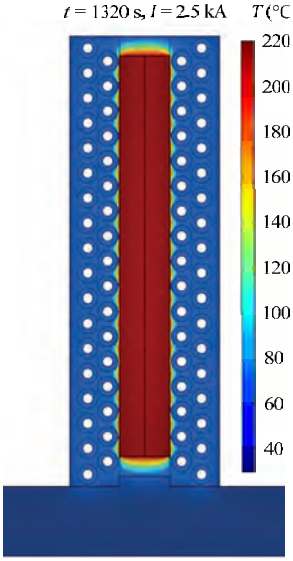

Fig. 19. Distribution of temperature T in the system after $t = 1320$ s of the heating process for $I = 2.5$ kA.

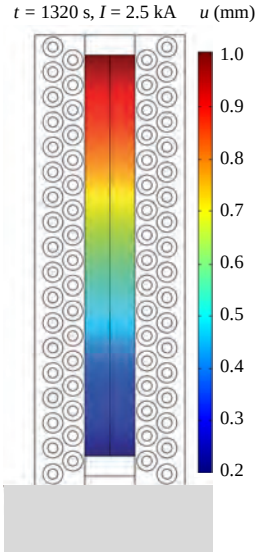

Fig. 20. Distribution of displacements u in the disk after $t = 1320$ s of the heating process for $I = 2.5$ kA.

It can be seen that the overall temperature of the disk exceeded $200\,°C$ and displacement of the internal bore of the disk exceeded (along its whole length) the value of $\Delta r_{AB} = 0.2$ mm, which is enough for manufacturing the hrink fit.

Even more information is contained in Figs. 21 and 22 showing the time evolution of the average temperature of the disk and time evolution of the average displacement of the disk bore.

While the time evolution of the average temperature is almost linear (due to small heat losses in the system), the average displacement of the inner radius of the disk grows with very slightly growing gradient. This follows from a nonuniform distribution of mass of the disk along the growing radius and also from nonlinearities (with respect to the temperature) of its physical parameters.

The time of reaching the minimum dilatation of the internal bore of the disk can be reduced using higher amplitude of the field current. Preferred is, however, slower heating in order to avoid possible undesirable changes in the material structure.

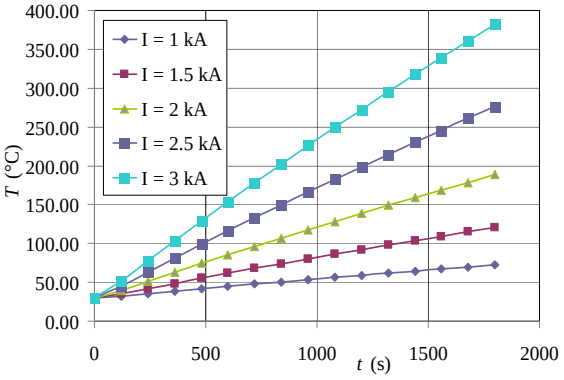

Fig. 21. Time evolution of average temperature T in the disk for various amplitudes I of the field current.

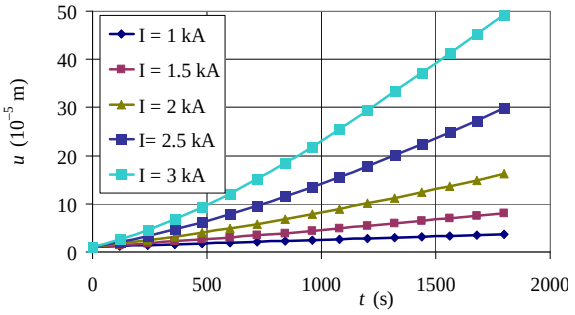

Fig. 22. Time evolution of average displacement u of the disk bore for various amplitudes I of the field current.

6. Conclusions

The results obtained are physically real and correspond to industrial experience. Nevertheless, we plan (in collaboration with some industrial plants because their realization is beyond the possibilities of academic workshops) their experimental verification. Further theoretical research must be aimed particularly at acceleration of the computation algorithms because the complete processing of one example takes about five hours. More attention will also be paid to the accuracy of the input data (temperature dependencies of physical parameters of various materials) because they often exhibit certain variances dependent on thein sources (databases, datasheets etc.).

7. Acknowledgments

This work was financially supported by the Grant project GACR P102/11/0498 and project SGS-2012-039 (University of West Bohemia).

References

1. V. Kotlan, P. Karban, B. Ulrych, I. Doležel, P. Kůs, Hard-Coupled Modeling of Induction Shrink Fit of Gas-Turbine Active Wheel // In Proc. ISTET'11. – Klagenfurt, Austria. – 2011. – P. 173–178.
2. B. Boley, J. Wiener, Theory of Thermal Stresses. – New York, USA: Wiley. – 1960.
3. M. Kuczmann, A. Iványi, The Finite Element Method in Magnetics. – Budapest, Hungary: Akadémiai Kiadó. – 2008.
4. J. Holman, Heat Transfer. – New York, USA: McGraw-Hill. – 2001.

ІНДУКЦІЙНА ТЕПЛОПРЕСОВА ПОСАДКА ДИСКА НА ВАЛ

Вацлав Котлан, Богуш Ульрих, Іво Долежел

Представлено повну модель індукційної теплопресової посадки диска на вал. Модель включає розрахунок різниці діаметра вала та внутрішнього діаметра диска, перевірку напруження фон Мізеса в диску та валі, поточкове зображення процесу індукційного нагрівання й визначення критичної швидкості обертання вала. Ілюстрацію методики здійснено на типовому прикладі.

Václav Kotlan – Ph.D., born in 1979, graduated from the Faculty of Electrical Engineering (University of West Bohemia in Pilsen, Czech Republic) in 2003. In 2008 he received his Ph.D. degree in the field of Electrical Power Engineering. His research interests are aimed at theoretical problems of electrical power systems (transmission line parameters, numerical methods for analysis of transient phenomena on transmission lines) and in the last years he has also dealt with numerical solution of electromagnetic and coupled fields. He published about 50 papers in scientific journals and conference proceedings.

Bohuš Ulrych – Ph.D., Associate Professor, born in 1937, works in the Department of Theory of Electrical Engineering at the Faculty of Electrical Engineering of the University of West Bohemia in Pilsen, Czech Republic. His professional interests are aimed at modern numerical methods for solution of physical fields and engineering applications. He is an author or co-author of about 250 papers, several books and textbooks, and a lot of software for teaching and calculation of electromagnetic fields and coupled problems.

Ivo Doležel – Ph.D., Professor, born in 1949, obtained his Engineering degree from the Faculty of Electrical Engineering (Czech Technical University in Prague, Czech Republic) in 1973. Presently he works with the Czech Technical University in Prague, Academy of Sciences of the Czech Republic (Institute of Thermomechanics) in Prague and with the University of West Bohemia in Pilsen.

His interests are aimed mainly at mathematical and computer modeling of electromagnetic fields and coupled problems in heavy current and power applications. He is an author or co-author of two monographs (USA), about 400 research papers and several large codes.